Innovations in Piezoelectric Shunt Damping

A.J. Fleming*, S. Behrens, S.O.R. Moheimani.
Department of Electrical and Computer Engineering
The University of Newcastle, Australia

ABSTRACT

Piezoelectric transducer (PZT) patches can be attached to a structure in order to reduce vibration. The PZT patches essentially convert vibrational mechanical energy into electrical energy. The electrical energy can be dissipated via an electrical impedance. Currently, impedance designs require experimental tuning of resistive circuit elements to provide optimal performance. A systematic method is presented for determining the resistance values by minimizing the $\mathcal{H}_2$ norm of the damped system. After the design process, shunt circuits are normally implemented using discrete resistors, virtual inductors, and Riordian Gyrators. The difficulty in constructing the shunt circuits and achieving reasonable performance has been an ongoing and unaddressed problem in shunt damping. A new approach to implementing piezoelectric shunt circuits is presented. A synthetic impedance, consisting of a voltage controlled current source and DSP system, is used to synthesize the terminal impedance of a shunt network. A two mode shunt circuit is designed and implemented for an experimental simply supported beam. The second and third structural modes of the beam are reduced in magnitude by 22 and 18 dB.

Keywords: Piezoelectricity, Piezoelectric, Laminate, Shunt, Damping, Resistor, Optimization, Network, Synthesis.

1. INTRODUCTION

Today's increasingly high speed and lightweight structures are subject to extensive vibrations that can reduce structural life and contribute to mechanical failure. Piezoelectric transducers (PZT's) in conjunction with appropriate circuitry, can be used as a mechanical energy dissipation device. By placing an electrical impedance across the terminals of the PZT, the passive network is capable of damping structural vibrations. If a simple resistor is placed across the terminals of the PZT, the PZT will act as a viscoelastic damper[1] . If the network consists of a series inductor-resistor $R-L$ circuit, the passive network combined with the inherent capacitance of the PZT creates a damped electrical resonance. The resonance can be tuned so that the PZT element acts as a tuned vibrational energy absorber[1] . This damping methodology is commonly referred to as passive shunt damping. Passive shunt damping is regarded as a simple, low cost, light weight, and easy to implement method of controlling structural vibrations. A desirable property of passive shunt damping is that the controlled system is guaranteed to be stable in the presence of structural uncertainties.

Flexible mechanical structures have an infinite number of resonant frequencies (or structural modes). If the tuned energy absorber[1] is used to minimize the vibration of a number of modes, one would need an equal number of PZT patches and shunting circuits. This is clearly impractical. Wu[2] reports a method of damping multiple vibration modes using a single PZT. The proposed circuit includes a "current blocker" consisting of a parallel capacitor-inductor network placed in series with each $R-L$ shunt circuit designed for one structural mode. Depending on the number of structural modes to be shunt damped simultaneously, a different number of $C-L$ networks are placed in series with the parallel $R-L$ shunt branch.

Although shunt damping circuits have a fixed structure, the designer is still faced with the problem of choosing component values. The blocking circuit and branch inductance values are easily found using classical circuit theory and the resonant frequencies of the structure. Currently, damping resistors are determined experimentally by observing the frequency response of the damped system and varying the resistances to achieve a desirable trade off between peak reduction and side lobe amplitude[3,4,5,6,2,7,8] . An optimization technique is proposed that minimizes the $\mathcal{H}_2$ norm of the damped system. This provides a systematic and reliable method for designing the resistance values of shunt damping circuits.

There are also a number of implementation problems associated with single and multi-mode shunt damping techniques. PZT shunt circuits typically require large inductance values. Therefore, virtual inductors are required to

*Correspondence: Email ajf203@alinga.newcastle.edu.au; Phone: +61 2 4921 7223.

implement the inductor elements. Virtual inductors are large in size and sensitive to component variations and non-ideal characteristics. PZT shunt circuits are capable of generating large voltages for moderate structural excitations. This requires that the virtual inductor circuits be constructed from high voltage operational amplifiers. At least 30 high voltage opamps are required to damp three structural modes[†]. This paper introduces a method of implementing a specified shunt circuit with arbitrary order and complexity. The "synthetic impedance" uses a voltage dependant current source and DSP system to implement the terminal impedance of an arbitrary shunt network. It replaces physical circuits to provide effective structural damping without the problems encountered with direct circuit implementations.

2. PIEZOELECTRIC DEVICES

Piezoelectric devices have shown promising applications in active, semi-active, and passive vibration control[9] . Piezoelectric materials convert mechanical strains into electrical energy and vice versa. This characteristic can be exploited, allowing them to be used as both sensors and actuators.

2.1. Piezoelectricity

Piezoelectricity was discovered by Pierre and Jacques Curie in 1880. It is the phenomenon in which certain crystalline substances develop an electric field when subjected to pressure/forces, or conversely, exhibit a mechanical deformation when subjected to an electric field. This reciprocal coupling between mechanical and electrical energy renders piezoelectric materials useful in many applications including active, semi-active and passive vibration control.

The piezoelectric effect is found only in crystals having no center of symmetry. Examples include quartz, Rochelle Salt and synthetic polycrystalline ceramics; polyvinylflouride (PVDF) and lead-zirconate-titanate (PZT). The last two are commonly used in vibration control.

The piezoelectric effect is based on the elastic deformation of electric dipoles in a materials crystal lattice. If an external mechanical force deforms the crystal, an electric field and hence a charge distribution at the crystal's surface is generated. This phenomenon is termed the direct piezoelectric effect or "sensory effect". Applying an electrical field causes a deformation of the dipoles, leading to a constant volume strain of the crystal. This is termed the inverse piezoelectric or "actuator effect".

2.2. Piezoelectric Modeling

Piezoelectric crystals have a three-dimensional structure, i.e. crystal deformation occurs in 3 dimensions. Practical mechanical uses only require the effect in one or two dimensions, this can be approximated by manufacturing piezoelectric patches with large length and width to thickness ratios.

Piezoelectric transducers behave electrically like a capacitor C_p and mechanically like a stiff spring[10] . It is common practice to model the piezoelectric element as a capacitor C_p in series with a strain dependant voltage source[4] . The piezoelectric model is shown in Figure 3 (a).

3. PIEZOELECTRIC SHUNT DAMPING

Shunt damping methodologies are often grouped into two broad categories: single mode and multi-mode. Single mode shunt damping techniques are simple but damp only one structural mode for every PZT. Multiple mode shunt damping techniques require more complicated shunt circuits but are capable of damping many modes.

3.1. Single Mode Shunt Damping

Single mode damping was introduced to decrease the magnitude of one structural mode[4] . Two examples of single mode damping are shown in Figure 1 , parallel and series shunt damping. An $R-L$ shunt circuit circuit introduces an electrical resonance. This can be tuned to one structural mode in a manner analogous to a mechanical vibration absorber. Single mode damping can be applied to reduce several structural modes with the use of as many piezoelectric patches and damping circuits.

Problems may result if these piezoelectric patches are bonded to, or imbedded in the structure. First, the structure may not have sufficient room to accommodate all of the patches. Second, if there is insufficient room, the structure may be altered or weakened when the piezoelectric patches are applied. In addition, a large number of patches can increase the structural weight, making it unsuitable for applications such as aerospace.

[†]Based on a series circuit configuration with current blocker's in every branch, as shown in[2] .

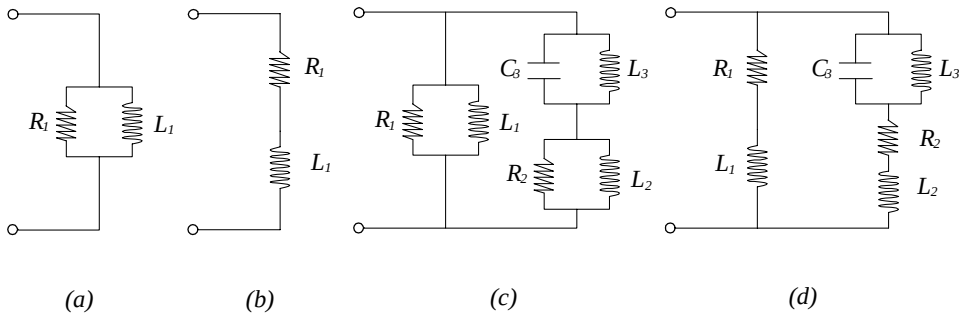

Figure 1. Examples of shunt circuits. Single mode: (a) parallel case, (b) series case. Multi-mode: (c) parallel case[2] , (d) series case.

3.2. Multiple Mode Shunt Damping

To alleviate the problems associated with single mode damping, multi-mode shunt damping has been introduced; i.e. the use of one piezoelectric patch to damp several structural modes. There are two common circuit configurations for multi-mode shunt damping, parallel and series. Examples of these two configurations are shown in Figure 1. There are other examples of multi-mode shunt damping but these will not be discussed in this paper.

The principle of multi-mode shunt damping is to insert a "current blocking" circuit[6,2,7,8] in series with each shunt branch. In Figure 1, the blocking circuit consists of a capacitor and inductor in parallel , $C_3 - L_3$. The number of antiresonant circuits in each $R - L$ shunt branch depends on the number of structural modes to be damped simultaneously. Each $R - L$ shunt branch is designed to dampen only one structural mode. For example, $R_1 - L_1$ in Figure 1 (c) is tuned to resonate at ω_1, the resonant frequency of the first structural mode to be damped. $R_2 - L_2$ is tuned to ω_2, the second structural mode to be damped, and so on.

According to Wu[2] , the inductance values for the shunt circuits shown in Figure 1 (c) and (d) can be calculated from the following expressions. It is assumed that $\omega_1 < \omega_2$.

$$L_1 = \frac{1}{\omega_1^2 C_p} \qquad L_2 = \frac{\left(L_1\tilde{L}_2 + \tilde{L}_2 L_3 - L_1 L_3 - \omega_2^2 L_1 \tilde{L}_2 L_3 C_3\right)}{\left(L_1 - \tilde{L}_2\right)\left(1 - \omega_2^2 L_3 C_3\right)} \qquad \text{where } \tilde{L}_2 = \frac{1}{\omega_2^2 C_p},\ L_3 = \frac{1}{\omega_1^2 C_3}$$

where C_p is the capacitance of the PZT, and C_3 is an arbitrary capacitor used in the current blocking network. In the following Sections C_3 will be taken as 100 ηF.

3.3. Implementation Difficulties

Currently shunt damping circuits are implemented using a network of physical components. There are a number of problems associated with this *direct circuit* implementation, the foremost of which are listed below.

- Typically the shunt circuits require large inductor values (up to thousands of Henries). Virtual grounded and floating inductors (Riordan gyrators[11]) are required to implement the inductor elements. Such virtual implementations are typically poor representations of ideal inductors. They are large in size, difficult to tune, and are sensitive to component age, temperature, and non-ideal characteristics.
- Piezoelectric patches are capable of generating hundreds of volts for moderate structural excitations. This requires the entire circuit to be constructed from high voltage components. Further voltage limitations arise due to the internal gains of the virtual inductors.
- The minimum number of opamps required to implement the shunt damping circuit increases rapidly with the number of modes to be damped. At least 30 opamps are required to mplement a series configuration multi-mode shunt damping circuit with current blocker's in every branch. The relationship between the number of opamps and the number of modes to be damped for this circuit configuration is given by $Opamps = 2n + 4n(n-1)$, where n is the number of modes to be damped.

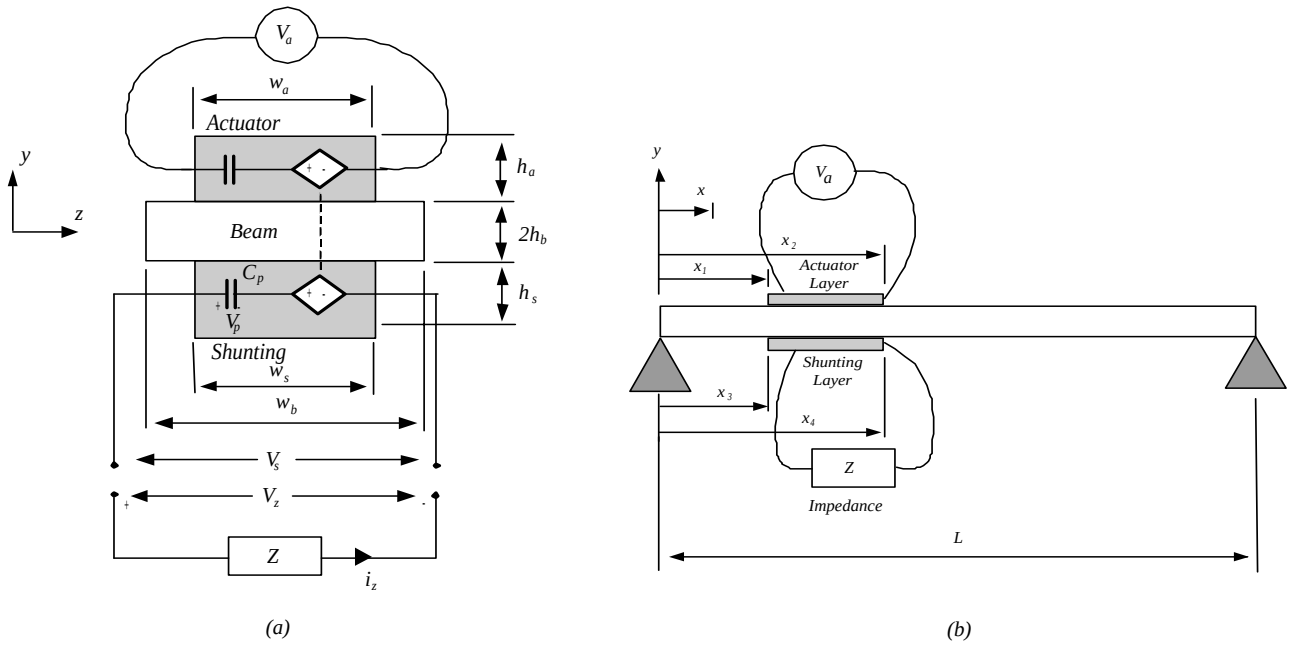

Figure 2. (a) Cross-section of the beam with piezoelectric laminate present; (b) The piezoelectric laminated simply-supported beam.

4. MODELLING THE COMPOUND SYSTEM

In this Section we sketch how the dynamics of a simply-supported piezoelectric laminate beam as illustrated in Figure 2 can be derived. Two piezoelectric patches are bonded to the structure using a strong adhesive material. One PZT will be used as an actuator to generate a disturbance and the other as a passive shunting layer. The subscripts "a", "b" and "s" correspond respectively to the actuating piezoelectric layer, the beam, and the shunting piezoelectric layer.

4.1. Structural Dynamics of a Simply Supported Beam

When modeling the dynamics of a structure, it is common practice to derive the transfer function between the displacement at any point along the beam and the actuator voltage, i.e., $Y(x,s)/V_a(s)$, and also the transfer function between the shunting piezoelectric voltage and the actuator voltage $V_s(s)/V_a(s)$.

The elastic deflection of a simply supported beam is described by the one dimensional Bernoulli-Euler beam equation which has been modified[12] as shown below:

$$\frac{\partial^2}{\partial x^2}\left[EI\frac{\partial^2 y(x,t)}{\partial x^2} - C_a v_a(x,t)\right] + \rho A\frac{\partial^2 y(x,t)}{\partial t^2} = 0 \tag{1}$$

where E, I, A and ρ represent the Young's modulus, moment of inertia, cross-sectional area and linear mass density of the beam respectively. The additional term is due to the moment applied to the neutral axis of the beam by the actuator piezoelectric layer, i.e., $M_a = C_a v_a(x,t)$ where C_a is a constant dependent on the actuator properties [13,14,15] . It is assumed that each piezoelectric patch is very thin and that the beam deflects only in the y axis. Simply supported boundary conditions imply $y(0,t) = y(L,t) = 0$ and $EI\frac{\partial y(0,t)}{\partial x} = EI\frac{\partial y(L,t)}{\partial x} = 0$.

By using the *modal analysis technique*[16] the position function $y(x,t)$, can be expanded as an infinite series of the form $y(x,t) = \sum_{i=1}^{\infty}\phi_i(x)q_i(t)$, where $\phi_i(x)$ are the normalized mode shapes given by $\phi_i(x) = \sqrt{\frac{2}{\rho AL}}\sin\left(\frac{i\pi x}{L}\right)$[16] , and $q_i(t)$ are the modal displacements[12] .

To formulate the dynamical response of the system, the Lagrange equations[16] are used to find the differential equation corresponding to each mode.

$$\ddot{q}_i(t) + \omega_i^2 q_i(t) = C_a[\phi_i'(x_1) - \phi_i'(x_2)]v_a(t) \tag{2}$$

The PZT sensor voltage can be described by $v_s(t) = C_s \left.\frac{\partial y(x,t)}{\partial x}\right|_{x_3}^{x_4}$ where C_s is the piezoelectric constant of the PZT[12] . In the sequel we will use the notation $(\bullet)'$, $(\dot{\bullet})$ to represent the derivatives with respect to the spatial variable x, and time t, respectively. The resonant frequencies ω_i are given by $\omega_i = \left(\frac{i\pi}{L}\right)^2 \sqrt{\frac{EI}{\rho A}}$.

The dynamic response is found by taking the Laplace transform of the above equation and substituting $Y_i(x,s) = \phi_i(x)q_i(s)$.

$$\frac{Y(x,s)}{V_a(s)} = \sum_{i=1}^{\infty} \frac{C_a[\phi_i'(x_1) - \phi_i'(x_2)]\phi_i(x)}{s^2 + 2\zeta_i w_i s + w_i^2}. \tag{3}$$

The above equation describes the elastic deflection of the entire flexible beam due to a voltage applied to the piezoelectric actuator. Note that the additional terms $2\zeta_i w_i s$, are added to compensate for structural damping and are usually found experimentally. The shunting layer voltage can be expressed as $v_s(t) = C_s \sum_{i=1}^{\infty} q_i(t)(\phi_i'(x_3) - \phi_i'(x_4))$. By taking the Laplace transform, the transfer function from the actuator to shunt voltage is found to be[17] ,

$$\frac{V_s(s)}{V_a(s)} = \sum_{i=1}^{\infty} \frac{C_s C_a[\phi_i'(x_1) - \phi_i'(x_2)][\phi_i'(x_3) - \phi_i'(x_4)]}{s^2 + 2\zeta_i w_i s + w_i^2}. \tag{4}$$

Then state-space model for $Y(x,s)/V_a(s)$ and $V_s(s)/V_a(s)$ can be represented as

$$\begin{aligned} \dot{\mathbf{x}}_b &= \mathbf{A}\mathbf{x}_b + \mathbf{B}V_a \\ Y &= \mathbf{C}_Y \mathbf{x}_b \\ V_s &= \mathbf{C}_{V_s} \mathbf{x}_b \end{aligned} \tag{5}$$

where x_b is the beam state vector, $\mathbf{C}_Y$ and $\mathbf{C}_{V_s}$ depend on the $Y(x,s)$ and $V_s(s)$.

4.2. Compound Dynamics

As discussed in Section 3.2, there are two common circuit configurations used for multi-mode shunt damping, series and parallel as shown in Figure 1. In order to model the presence of the shunt network, the coupled terminal dynamics of the circuit and laminated beam are considered.

Piezoelectric transducers behave electrically like a capacitor C_p and mechanically like a stiff spring. It is common to model the piezoelectric element as a capacitor C_p in series with a strain dependant voltage source[1,18] . Consider Figures 2 and 3 (a), where a piezoelectric patch is shunted with an impedance Z. The current-voltage relation of the impedance can be represented in state-space form as

$$\dot{\mathbf{x}}_z = \mathbf{A}_z \mathbf{x}_z + \mathbf{B}_z V_z \tag{6}$$

$$i_z = \mathbf{C}_z \mathbf{x}_z + \mathbf{D}_z V_z \tag{7}$$

where V_z is the voltage across the impedance and i_z is the current flowing through the circuit. The relationship between V_z and V_p, shown in Figures 2 and 3 (a), is

$$\dot{\mathbf{x}}_b = \mathbf{A}\mathbf{x}_b + \mathbf{B}V_z \tag{8}$$

$$V_p = -\mathbf{C}_{V_s} \mathbf{x}_b \tag{9}$$

where V_p is the voltage induced from the electromechanical coupling effect. By shunting the piezoelectric patch, the voltage V_z across the shunting layer or impedance, shown in Figure 3 (a), is related to the terminal voltage and current by,

$$V_z = V_p - \frac{1}{C_p} \int i_z dt \tag{10}$$

The variable i_z, can be replaced with $\dot{\mathbf{q}}_z$, the charge on the PZT. Consequently, by replacing V_z and substituting $V_p = -\mathbf{C}_{V_s}\mathbf{x}_b$ (6), (7) and (8) becomes,

$$\begin{bmatrix} \dot{\mathbf{x}}_b \\ \dot{\mathbf{x}}_z \\ \dot{\mathbf{q}}_z \end{bmatrix} = \begin{bmatrix} \mathbf{A} - \mathbf{B}\mathbf{C}_{V_s} & \mathbf{0} & -\frac{1}{C_p}\mathbf{B} \\ -\mathbf{B}_z\mathbf{C}_{V_s} & \mathbf{A}_z & -\frac{1}{C_p}\mathbf{B}_z \\ -\mathbf{D}_z\mathbf{C}_{V_s} & \mathbf{C}_z & -\frac{1}{C_p}\mathbf{D}_z \end{bmatrix} \begin{bmatrix} \mathbf{x}_b \\ \mathbf{x}_z \\ \mathbf{q}_z \end{bmatrix}. \tag{11}$$

If a voltage V_a is applied to the actuator PZT, then (11) becomes,

$$\begin{aligned} \dot{\mathbf{X}} &= \tilde{\mathbf{A}}\mathbf{X} + \tilde{\mathbf{B}}V_a \\ V_z &= \tilde{\mathbf{C}}_{V_s}\mathbf{X} \\ Y &= \tilde{\mathbf{C}}_Y\mathbf{X}. \end{aligned} \tag{12}$$

where $\mathbf{X} = \begin{bmatrix} \mathbf{x}_b & \mathbf{x}_z & \mathbf{q}_z \end{bmatrix}^T$, $\tilde{\mathbf{B}} = \begin{bmatrix} \mathbf{B} & \mathbf{0} & \mathbf{0} \end{bmatrix}^T$, $\tilde{\mathbf{C}}_{V_s} = \begin{bmatrix} \mathbf{C}_{V_s} & \mathbf{0} & \mathbf{0} \end{bmatrix}^T$, $\tilde{\mathbf{C}}_Y = \begin{bmatrix} \mathbf{C}_Y & \mathbf{0} & \mathbf{0} \end{bmatrix}^T$ and

$$\tilde{\mathbf{A}} = \begin{bmatrix} \mathbf{A} - \mathbf{B}\mathbf{C}_{V_s} & \mathbf{0} & -\frac{1}{C_p}\mathbf{B} \\ -\mathbf{B}_z\mathbf{C}_{V_s} & \mathbf{A}_z & -\frac{1}{C_p}\mathbf{B}_z \\ -\mathbf{D}_z\mathbf{C}_{V_s} & \mathbf{C}_z & -\frac{1}{C_p}\mathbf{D}_z \end{bmatrix}.$$

5. DETERMINING THE SHUNTING RESISTANCES VIA OPTIMIZATION

In order to find appropriate values for the shunt resistors $\mathbf{R} = \{R_1, R_2, ..., R_n\}$ an optimization approach is proposed; a set of resistors can be found so that the $\mathcal{H}_2$ norm of the damped system is minimized. Minimizing the $\mathcal{H}_2$ norm of the system minimizes the RMS displacement at a single, or series of points due to a spectrally white disturbance signal applied to the actuator(s).

5.1. Optimization Technique

Consider a transfer function matrix $\tilde{\mathbf{G}}(s) \in \mathbb{C}^{m\times n}$ representing the damped system (12). The $\mathcal{H}_2$ norm of $\tilde{\mathbf{G}}(s)$, denoted $\left\|\tilde{\mathbf{G}}(s)\right\|_2$, is defined as:

$$\left\|\tilde{\mathbf{G}}(s)\right\|_2^2 = \frac{1}{2\pi}\int_{-\infty}^{\infty} tr\left(\tilde{\mathbf{G}}^T(-j\omega)\tilde{\mathbf{G}}(j\omega)d\omega\right)$$

Let $\tilde{\mathbf{G}}(s)$ have the realization $\tilde{\mathbf{G}}(s) = \tilde{\mathbf{C}}(s\mathbf{I} - \tilde{\mathbf{A}})^{-1}\tilde{\mathbf{B}}$. If the matrix $\tilde{\mathbf{A}}$ is stable the following equality holds

$$J = \|\mathbf{G}(s)\|_2^2 = tr(\tilde{\mathbf{C}}\mathbf{P}\tilde{\mathbf{C}}^T) \tag{13}$$

where $\mathbf{P}$ satisfies the *Lyapunov* equation $\tilde{\mathbf{A}}^T\mathbf{P} + \mathbf{P}\tilde{\mathbf{A}} + \tilde{\mathbf{B}}\tilde{\mathbf{B}}^T = \mathbf{0}$. In this case $\tilde{\mathbf{A}}$ is a function of $\mathbf{R}$. This leads to the following constrained optimization problem:

$$\mathbf{R}^* = \arg\min_{s.t.\ \mathbf{g}=\mathbf{0}} J \tag{14}$$

where $\mathbf{g} = \tilde{\mathbf{A}}^T\mathbf{P} + \mathbf{P}\tilde{\mathbf{A}} + \tilde{\mathbf{B}}\tilde{\mathbf{B}}^T$, and $\mathbf{R} = \{R_1, R_2, ..., R_n\}$, $R_1,\ R_2, ..., R_n > 0$.

Having set up the optimization problem (14), a number of methods can be employed to find an optimal set of resistors $\mathbf{R}^* = \{R_1^*, R_2^*, ..., R_n^*\}$. One such method is the Nelder-Mead simplex search alogorithm. A more elegant and computationally efficient method of solving (14) is use the gradient search algorithm. By introducing the matrix of Lagrange multipliers $\mathbf{S}$ the Lagrangian L is formed as follows

$$L = tr(\tilde{\mathbf{C}}\mathbf{P}\tilde{\mathbf{C}}^T) + tr(\mathbf{g}\mathbf{S}). \tag{15}$$

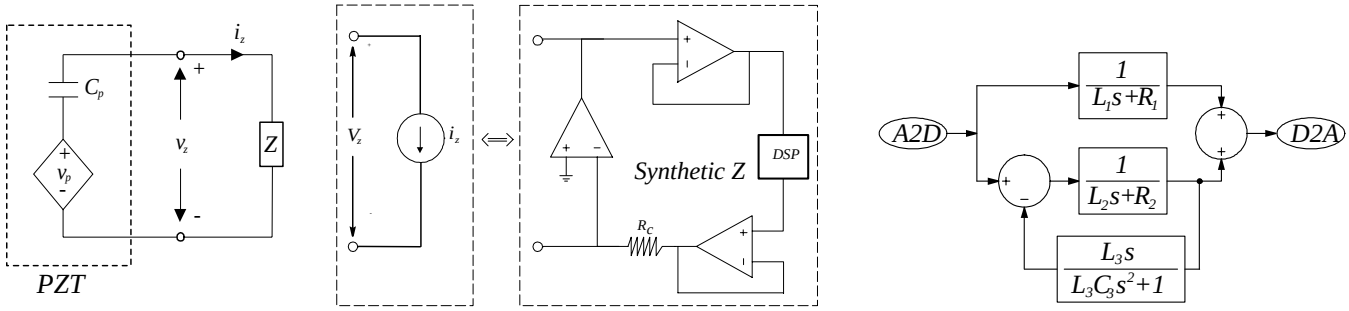

a) Shunted PZT schematic (b) Current Source Implementation (c) Admittance transfer function

Figure 3.

The first order necessary conditions for optimality are found by equating the derivatives of L with respect to the parameters $\mathbf{P}$, $\mathbf{S}$ and $\mathbf{R}$ to zero,

$$\frac{\partial L}{\partial \mathbf{S}} = \tilde{\mathbf{A}}\mathbf{P} + \mathbf{P}\tilde{\mathbf{A}}^T + \tilde{\mathbf{B}}\tilde{\mathbf{B}}^T = \mathbf{0} \tag{16}$$

$$\frac{\partial L}{\partial \mathbf{P}} = \tilde{\mathbf{A}}^T\mathbf{S} + \mathbf{S}\tilde{\mathbf{A}} + \tilde{\mathbf{C}}^T\tilde{\mathbf{C}} = \mathbf{0} \tag{17}$$

$$\frac{\partial L}{\partial R_1} = tr\left(\tilde{\mathbf{E}}_1\mathbf{P}\mathbf{S} + \mathbf{P}\tilde{\mathbf{E}}_1^T\mathbf{S}\right) = 0$$

$$\vdots$$

$$\frac{\partial L}{\partial R_n} = tr\left(\tilde{\mathbf{E}}_n\mathbf{P}\mathbf{S} + \mathbf{P}\tilde{\mathbf{E}}_n^T\mathbf{S}\right) = 0 \tag{18}$$

With n resistors, $\tilde{\mathbf{A}}$ can be represented as $\tilde{\mathbf{A}} = \hat{\mathbf{A}} + R_1\tilde{\mathbf{E}}_1 + ... + R_n\tilde{\mathbf{E}}_n$, where $\hat{\mathbf{A}}$ is independent of $\mathbf{R}$.

The $\mathcal{H}_2$ norm of the system can now be minimized by solving the above equations simultaneously. It is not possible to obtain a closed form solution, so a numerical approach is required.

As preliminaries for the optimization, the static matrices ($\tilde{\mathbf{B}}$ and $\tilde{\mathbf{C}}$) are computed and an initial estimate $\mathbf{R}_0$ is made for $\mathbf{R}^*$. Matrix $\tilde{\mathbf{A}}$ is a function of $\mathbf{R}_k$ and is updated at each iteration Matrices $\mathbf{P}$ and $\mathbf{S}$, are calculated by solving the Lyapunov equations (16) and (17)**.** The direction of steepest descent is found by evaluating the gradient vector, whose entries are the partial derivatives of L with respect to $R_1, R_2, ..., R_n$ (18). The process is iterated by updating $\mathbf{R}_k$ until a minima is obtained (i.e. until the exiting conditions $\frac{\partial L}{\partial R_i} \approx 0$ and $L_{k+1} \approx L_k$ are satisfied).

6. IMPLEMENTATION OF SHUNT DAMPING CIRCUITS

It should be clear from previous sections that although the concept of multi-mode shunt damping is useful, implementation difficulties make its application somewhat limited. This section introduces a new method of implementing complicated shunt damping circuits using only a few opamps, one resistor, and a digital signal processor (DSP).

6.1. The Synthetic Impedance

We define a "synthetic impedance" as a two terminal device that establishes an arbitrary relationship between voltage and current at its terminals. The functionality is shown in Figure 3 (b), where $i_z(t) = f(v_z(t))$. This can be made to synthesize any network of physical components by fixing i_z to be the output of a linear transfer function of v_z. i.e.

$$I_z(s) = Y(s)V_z(s) \tag{19}$$

where $Y(s) \equiv \frac{1}{Z(s)}$ and $Z(s)$ is the impedance to be seen from the terminals.

6.2. Circuit Diagram / Transfer Function Interconnection Equivalence

In section 6.1, $Y(s)$ is formed analytically by calculating the complex admittance of the network. In practical situations where there may be a large number of shunt circuit elements, it is desirable to "redraw" the circuit as a transfer function block diagram so that the overall $\frac{output(s)}{input(s)}$ relationship is equal to $Y(s)$. This can simplify the process of writing DSP algorithms. Moreover, if a graphical compilation package such as the Real Time Workshop (RTW) for Matlab is available, the need for any transfer function derivations or algorithm coding is removed.

Two transformations of interest are shown in Figures 4. These can be combined to find an equivalent transfer function form for any network of impedances.

Parallel circuit equivalence. Consider the parallel network components $Z_1, Z_2, \ldots, Z_m$ as shown in Figure 4 (a). The terminal impedance and admittance of this network is

$$Z_T(s) = (\tfrac{1}{Z_1} + \tfrac{1}{Z_2} + \ldots + \tfrac{1}{Z_m})^{-1} \quad Y_T(s) = \tfrac{1}{Z_1} + \tfrac{1}{Z_2} + \ldots + \tfrac{1}{Z_m} \tag{20}$$

Now consider the transfer function block diagram, also shown in Figure 4 (a).

$$G(s) = \frac{T(s)}{R(s)} = \frac{1}{Z_1} + \frac{1}{Z_2} + \ldots + \frac{1}{Z_m} \tag{21}$$

It is noted that $Y_T(s)$ and $G(s)$, as described in equations (20) and (21) are identical. Therefore, if a synthetic impedance as shown in Figure 3 (b) is implemented with a transfer function equal to $G(s)$, the impedance seen from the terminals will be identical to the impedance of the parallel network shown in Figure 4 (a) (with impedance $Z_T(s)$ given by (20)).

Series circuit equivalence. Consider the series network components $Z_1, Z_2, \ldots, Zm$ as shown in Figure 4 (b). The terminal impedance and admittance of this network is:

$$Z_T(s) = Z_1 + Z_2 + \ldots + Z_m \quad Y_T(s) = \tfrac{1}{Z_1 + Z_2 + \ldots + Z_m} \tag{22}$$

Now consider the transfer function block diagram, also shown in Figure 4 (b)

$$G(s) = \tfrac{T(s)}{R(s)} = \tfrac{\frac{1}{Z_1}}{1 + \frac{1}{Z_1}Z_2 + \ldots + \frac{1}{Z_1}Z_m} \quad G(s) = \tfrac{1}{Z_1 + Z_2 + \ldots + Z_m} \tag{23}$$

It is noted that $Y_T(s)$ and $G(s)$ as described in equations (22) and (23) are identical. Therefore, if a synthetic impedance as shown in Figure 3 (b) is implemented with a transfer function equal to $G(s)$, the impedance seen from the terminals will be identical to the impedance of the series network shown in Figure 4 (b) (with impedance $Z_T(s)$ given by (22)).

6.3. Synthesis of Piezoelectric Shunt Damping Circuits

A synthetic impedance that implements the multi-mode shunt damping circuit shown in Figure 1 (d) will now be designed.

The implementing circuit is similar to the example implementation shown in Figure 3 (b). A voltage controlled current source constructed from a single opamp is used together with buffer/amplifiers and a DSP system to simulate an impedance. The two unity gain buffers are replaced with non-inverting amplifiers of gain $\frac{1}{10}$ and 10. This retains the functionality while allowing the DSP system to operate at a voltage 10 times lower than that dealt with by the current source and buffer/amplifiers. A voltage protection device is placed at the input to the DSP analog to digital converter. The only required high voltage components are now the buffer/amplifier and current source opamp. The resistor R_c sets the transconductance gain of the system. In order to minimize quantization error, a reasonable portion of the digital to analog converters range should be utilized. A larger resistor requires a larger voltage to provide a specified current. To maintain a unity transconductance, a gain equal to the value of the resistance R_c should be placed internally in the DSP algorithm or in series with a transfer function block diagram.

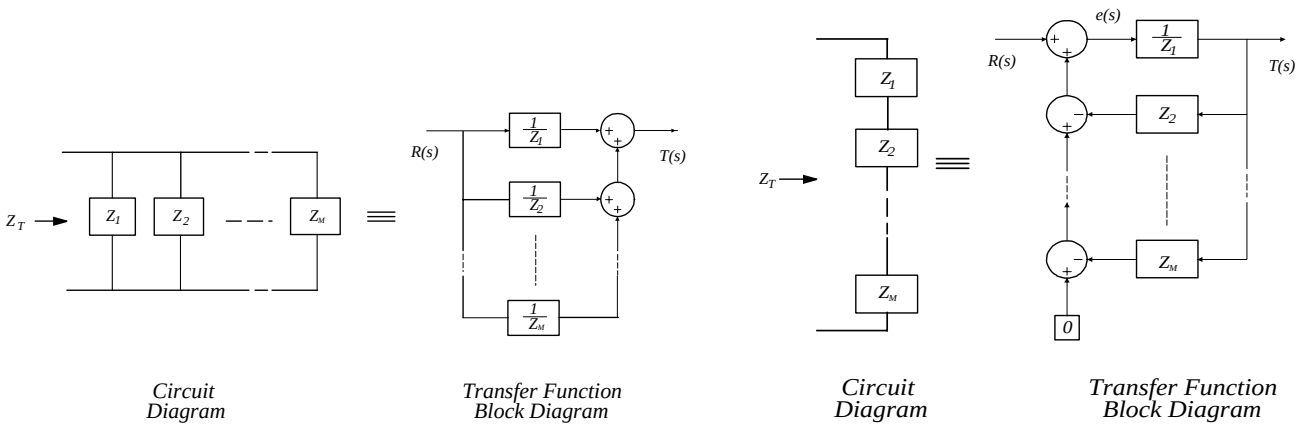

(a) Parallel equivalence (b) Series equivalence

Figure 4.

As discussed in Section 6.2 there are two approaches to designing the DSP algorithm. The first involves deriving the admittance transfer function of the network then implementing the time domain response on the DSP. The second approach, using a graphical compilation package does not require any derivations or coding and will be used here. The circuit of Figure 1 (d) is 'redrawn' in Simulink[‡] as a transfer function block diagram using the methods described in Section 6.2. The resulting Simulink block diagram is shown in Figure 3 (c). The Real Time Workshop for Matlab is now invoked to compile the Simulink diagram into executable code. This is downloaded onto the DSP hardware[§] and executed in real time. The sampling time of the digital system is 80 kHz.

7. EXPERIMENTAL RESULTS

To assess the merit of the concepts presented, a number of experiments were carried out on a simply supported piezoelectic laminate beam. By identifying the resonant frequencies and damping ratios of the beam, a 5 mode (10^{th} order) truncated model is constructed. The optimization technique described in Section 5.1 is then employed to determine the optimal shunt resistances. Finally, the optimal parallel and series shunt circuits are synthesized and applied to the structure. Damping performance is evaluated by measuring the free and damped frequency responses of the beam.

7.1. Experimental Setup

The experimental beam is a uniform aluminum bar with rectangular cross Section and experimentally pinned boundary conditions at both ends. A pair of piezoelectric ceramic patches (PIC151) are attached symmetrically to either side of the beam surface. One patch is used as an actuator and the other as a shunting layer. Experimental beam and piezoelectric parameters are summarized in Table 1.

The displacement and voltage frequency responses are measured using a Polytec laser vibrometer (PSV-300) and a HP spectrum analyzer (35670A). In both cases a swept sine excitation is applied to the actuator PZT.

The current source and buffer/amplifiers required for the synthetic impedance are constructed from Burr Brown OPA445 opamps. These opamps have a supply voltage limit of ± 45 v.

7.2. Optimization Results

In order to perform the optimization, an accurate model of the system is required. For obvious reasons the infinite order model produced by the modal analysis technique is not suitable for use in the optimization. As an alternative,

[‡]A graphical simulation environment for Matlab.

[§]The target processing hardware is the dSPACE ds1103 processing and I/O board.

Beam Parameters	
Length, L	$0.6\ m$
Width, w_b	$0.05\ m$
Thickness, h_b	$0.003\ m$
Youngs Modulus, E_b	$65 \times 10^9\ N/m^2$
Density, ρ	$2650\ kg/m^2$

PZT Parametes	
Length	$0.070\ m$
Charge Constant, d_{31}	$-210 \times 10^{-12}\ m/V$
Voltage Constant, g_{31}	$-11.5 \times 10^{-3}\ Vm/N$
Coupling Coefficient, k_{31}	0.340
Capacitance, C_p	$0.105\ \mu F$
Width, $w_s\ w_a$	$0.025\ m$
Thickness, $h_s\ h_a$	$0.25 \times 10^{-3}\ m$
Youngs Modulus, $E_s\ E_a$	$63 \times 10^9\ N/m^2$

Table 1. Parameters of the simply-supported piezoelectric laminated beam.

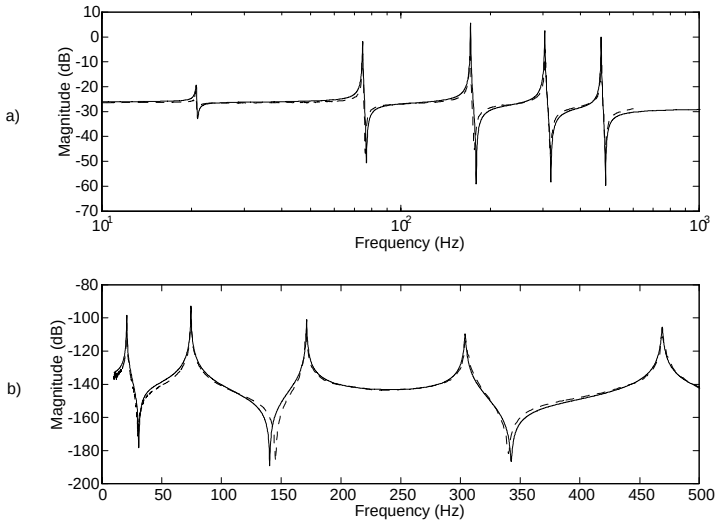

Figure 5. Frequency respnse of a) $\frac{V_s(s)}{V_a(s)}$, b) $\frac{d(0.170,s)}{V_a(s)}$. Experimental $(\cdots)$ modelled (—).

the displacement and voltage frequency responses are measured and used to tune a finite order model with the following structure:

$$\begin{aligned} G_{yv}(s) &= \frac{Y(0.170,s)}{V_a(s)} = \sum_{i=1}^{5} \frac{Fy_i}{s^2 + 2\zeta_i\omega_i s + \omega_i^2} + Ky_{opt} \\ G_{vv}(s) &= \frac{V_s(s)}{V_a(s)} = \sum_{i=1}^{5} \frac{Fv_i}{s^2 + 2\zeta_i\omega_i s + \omega_i^2} + Kv_{opt} \end{aligned} \tag{24}$$

where Ky_{opt} and Kv_{opt} are the zero frequency correction terms introduced in[17] . The frequency response of the experimental system and identified model is shown in Figure 5. It is observed that the identified model is a good representation of the true system over the bandwidth of interest.

Although the truncated model can be found to minimize the $\mathcal{H}_2$ norm of the additive error system[17] , the inherent feed through K_{opt} causes the $\mathcal{H}_2$ norm of the corrected system to approach infinity. To overcome this adverse effect, the corrected system $\left[\begin{array}{c|c} \mathbf{A}_c & \mathbf{B}_c \\ \hline \mathbf{C}_c & \mathbf{D}_c \end{array}\right]$ is remodelled with an additional parallel low pass filter $G_f(s) = \frac{\alpha}{s^2+2\zeta\omega_c s+\omega_c^2}$. If $\omega_c \gg \max(\omega_i)$, and $\frac{\alpha}{\omega_c^2} = K_{opt}$, the dynamics of the system in the bandwidth of interest are retained. The state space realization becomes:

$$\left[\begin{array}{cc|c} \mathbf{A}_c & 0 & \mathbf{B}c \\ 0 & \mathbf{A}_f & \mathbf{B}_f \\ \hline \mathbf{C}_c & \mathbf{C}_f & 0 \end{array}\right] \tag{25}$$

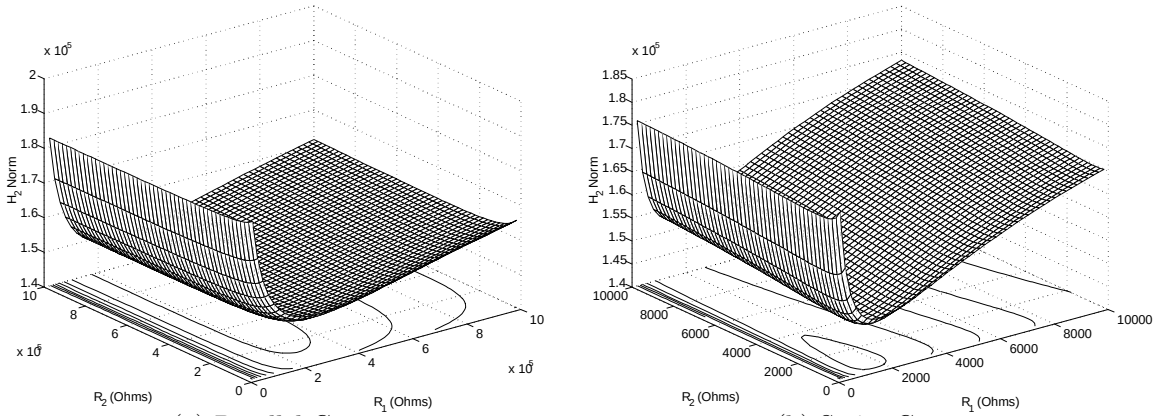

(a) Parallel Case (b) Series Case

Figure 6. $\mathcal{H}_2$ norm cost surface

a) **Experimental Results**		
	Parallel	Series
1st Mode Reduction	21 dB	22 dB
2nd Mode Reduction	18 dB	19 dB
$\frac{\text{Undamped Settling Time}}{\text{Damped Settling Time}}$	$\frac{1}{10}$	$\frac{1}{10}$

b) **Optimization Results**		
R_1	273.8 kΩ	1543.4 Ω
R_2	550.7 kΩ	550.7 Ω
L_1	43 H	43 H
L_2	20.9 H	20.9 H
$\hat{L}_2$	45.2 H	45.2 H

Table 2.

where $\left[\begin{array}{c|c} \mathbf{A}_f & \mathbf{B}_f \\ \hline \mathbf{C}_f & \mathbf{D}_f \end{array}\right]$ is the state space realization of the filter $G_f(s)$. Note that the feed through term $\mathbf{D}_c$ has been eliminated. Because the controller is of fixed structure, the dynamics of the introduced filter will not effect the optimization. The technique presented in Section 5.1 can now be applied.

With the aim of damping the second and third structural modes, the optimization is performed for both the series and parallel circuit configurations. The second and third modes are chosen for their high resonant peaks, and because the location of the PZT provides the greatest authority over these two modes. (See[19] for a discussion of PZT placement issues). The cost surfaces and a summary of the optimization results are shown in Figure 6, and Table 2 b).

In an earlier report where experimental tuning is performed[6] , Wu makes the observation that the parallel circuit is easier to tune. This claim is justified by Figure 6 that clearly show a greater sensitivity to resistance variations in the series cost surface.

7.3. Damping Performance

The optimized series and parallel shunt circuits are now applied to the beam. As shown in Section 6.3, the circuits are first converted into a transfer function block diagram, compiled with RTW, then downloaded onto the DSP hardware. The dSPACE ds1103 processing and I/O board was chosen as the target DSP hardware

Figure 7 (a) shows the theoretical and experimental damped frequency response. Figure 7 (b) shows the experimental time domain response to a filtered step disturbance (band pass filtered between 40 and 200 Hz). A summary of the performance is provided in Table 2 a).

It is noted that the same experiments have been performed using discrete resistors, virtual inductors, and Riordan gyrators[20] . Non-idealities in the virtual inductors result in a poor correlation between experimental and predicted frequency responses. Peak damping performance is 3 to 5 dB lower than that achieved here.

The synthetic impedance has proven to be a high performance method of implementing shunt damping circuits. It has a low number of high voltage components, is immune to component non-ideality, and requires no tuning of sensitive virtual circuits.

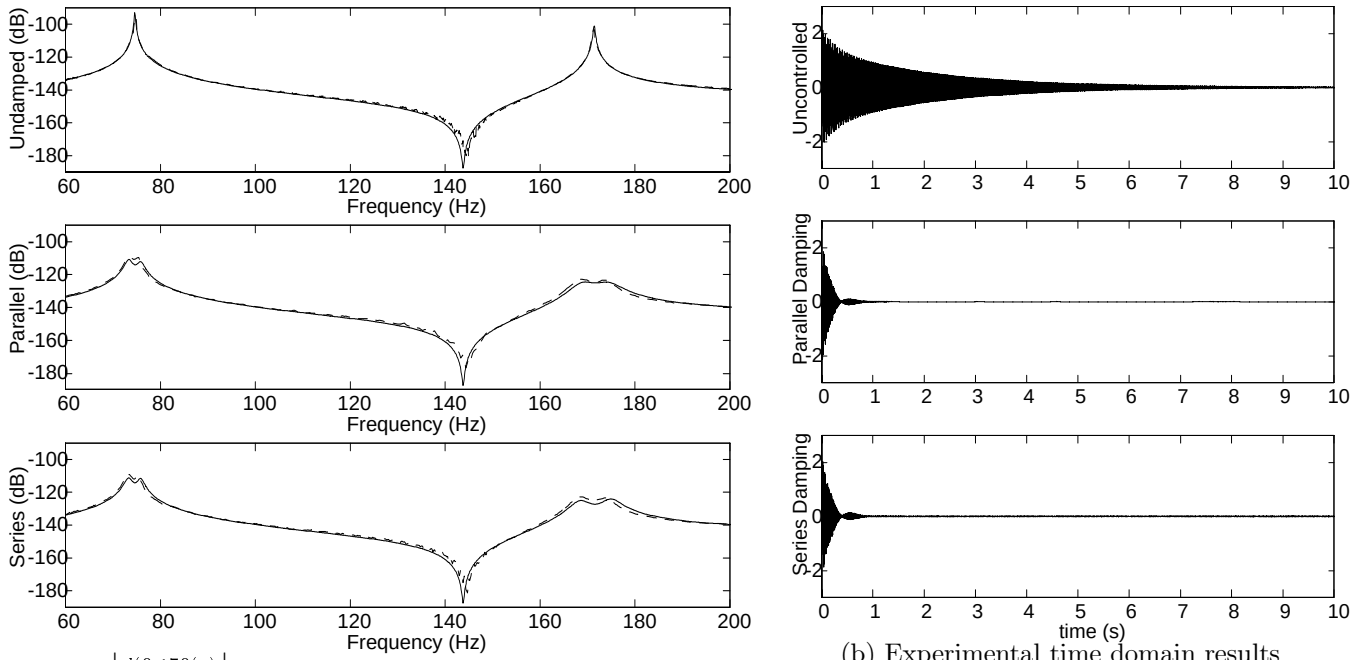

(a) $\left|\frac{d(0.170(s)}{V_a(s)}\right|$. Experimental $(\cdots)$ Theoretical (—)

(b) Experimental time domain results

Figure 7. Damping Performance.

8. CONCLUSIONS

Modern high performance design specifications have given rise to the widespread use of lightweight structures. These structures are prone to undesirable resonant vibrations that can reduce structural life and contribute to mechanical failure. Considerable research has been undertaken with the aim of damping these vibrations using a piezoelectric transducer and shunt damping circuit. Results to date have been encouraging but have lacked a systematic solution and practical implementation.

Previous design techniques have relied on the experimental tuning of circuit parameters to provide adequate performance. By modelling the compound system, an optimization problem has been formulated that minimizes the $\mathcal{H}_2$ norm of the resulting system. This provides a systematic procedure for designing fixed structure shunt damping circuits.

Previous shunt damping methodologies have also suffered from issues relating to the difficulty in implementing the shunt network. A synthetic impedance has been presented that implements the terminal impedance of a specified shunt network.

The concepts presented have been experimentally verified with good results. The modal resonant magnitudes have been reduced by up to 22 dB, this corresponds to a damped settling time $\frac{1}{10}^{\text{th}}$ that of the free response[¶] In general, theoretical predictions have been coherent with experimental results.

Future work will involve remodelling the shunt damping problem in a feedback control systems perspective. This is now possible as an impedance of arbitrary structure can be implemented.

ACKNOWLEDGEMENTS

This research was supported by the Centre for Integrated Dynamics and Control (CIDAC) and the Australian Research Council (ARC).

[¶]For the excitation described in Section 7.3.

REFERENCES

1. N. W. Hagood and A. V. Flotow, "Damping of structure vibrations with piezoelectric materials and passive electrical networks," *Journal of Sound and Vibration* **14**(2), p. 243, 1991.
2. S. Y. Wu, "Method for multiple mode shunt damping of structural vibration using a single pzt transducer," *Proceedings SPIE: Smart Structure and Materials 1993: Smart Structures and Intelligent System* **3327**, pp. 159–168, March 1998.
3. D. L. Edberg, A. S. Bicos, C. M. Fuller, J. J. Tracy and J. S. Fechter, "Theoretical and experimental studies of a truss incorporating active members," *Journal of Intelligent Materials Systems and Structures* **3**, p. 333, 1992.
4. N. W. Hagood and E. F. Crawley, "Experimental investigations of passive enhancement of damping space structures," *Journal of Guidance, Control and Dynamics* **14**(6), p. 1100, 1991.
5. J. J. Hollkamp, "Multimode passive vibration suppression with piezoelectric materials and resonant shunts," *Journal of Intelligent Materials Systems and Structures* **5**, p. 4, 1994.
6. S. Y. Wu, "Piezoelectric shunts with parallel R-L circuit for smart structural damping and vibration control," *Proceedings SPIE: Smart Structures and Materials 1996: Passive Damping and Isolation* **2720**, pp. 259–269, March 1996.
7. S. Y. Wu, "Multiple PZT transducer implemented with multiple-mode piezoelectric shunt for passive vibration damping," *Proceedings SPIE: Smart Structures and Materials 1999: Passive Damping and Isolation* **3672**, pp. 112–122, March 1999.
8. S. Y. Wu and A. S. Bicos, "Structure vibration damping experiments using improved piezoelectric shunts," *Proceedings SPIE: Smart Structures and Materials 1997: Passive Damping and Isolation* **3045**, pp. 40–50, March 1997.
9. K. W. Wang, "Structural vibration suppression via parametric control actions - piezoelectric materials with real-time semi-active networks.," *Series on Stability, Vibration and Control of Structures* **1**, pp. 112–134, 1995.
10. B. Clephas, *Adaptronics and Smart Structures - Basics, Material, Design, and Applications*, ch. 6.2, p. 106. Springer, 1999.
11. R. H. S. Riodan, "Simulated inductors using differential amplifiers," *Electron. Lett.* **3**(2), pp. 50–51, 1967.
12. C. R. Fuller, S. J. Elliott and P. A. Nelson, *Active Control of Vibration*, Academic Press, 1996.
13. H. R. Pota and T. E. Alberts, "Multivariable transferunctions for a slewing piezoelectric laminated beam," *ASME Journal of Dynamics Systems* **117**, pp. 353–359, 1995.
14. T. E. Alberts, T. V. DuBois and H. R. Pota, "Experimental verification of transfer functions for a slewing piezoelectric laminate beam," *Contr. Eng. Practice* **3**(2), pp. 163–170, 1995.
15. T. E. Alberts and J. A. Colvin, "Observations on the nature of transfer functions for control of piezoelectric laminates," *Journal of Intelligent Material Systems and Structures* **8**(5), pp. 605–611, 1991.
16. L. Meirovitch, *Elements of Vibration Analysis*, McGraw-Hill, Sydney, 2nd ed., 1996.
17. S. O. R. Moheimani, "Experimental verification of the correction transfer function of a piezoelectric laminated beam," *IEEE Transactions on Control Systems Technology* **8**, pp. 660–666, July 2000.
18. J. J. Dosch, D. J. Inman and E. Garcia, "A self-sensing piezoelectric actuator for collocated controller," *Journal of Intelligent Material Systems and Structures* **3**, pp. 166–185, January 1992.
19. S. O. R. Moheimani and T. Ryall, "Considerations in placement of piezoceramic actuators that are used in structural vibration control," *In Proc. IEEE Conference on Decision and Control* , pp. 1118–1123, December 1999.
20. S. Behrens and S. O. R. Moheimani, "Optimal resistive elements for multiple mode shunt-damping of a piezoelectric laminate beam," Technical Report EE0015, Department of Electrical and Computer Engineering, The University of Newcastle, March 2000. Also, to apper in the Proceedings of IEEE CDC2000, Sydney, Australia.